Pressure-induced phase transitions in α-$ZrMo_2O_8$

D. V. S. Muthu,[1,2] B. Chen,[1] J. M. Wrobel,[1] A. M. Krogh Andersen,[3] S. Carlson,[3] and M. B. Kruger[1]
[1]*Department of Physics, University of Missouri, Kansas City, Missouri 64110*
[2]*Department of Physics, Indian Institute of Science, Bangalore-560 012, India*
[3]*Inorganic Chemistry, Lund University, SE-22100 Lund, Sweden*
(Received 9 April 2001; revised manuscript received 26 July 2001; published 3 January 2002)

We report high-pressure Raman, infrared (IR), and optical-absorption spectra of α-$ZrMo_2O_8$ (trigonal) up to 38 GPa at room temperature. The spectroscopic studies are consistent with diffraction results that show that α-$ZrMo_2O_8$ transforms into δ-$ZrMo_2O_8$ (monoclinic) at about 1 GPa and the δ phase converts to the ε phase (triclinic) at about 2.0 GPa. Optical-absorption measurements give an estimate of the band gap of about 0.6 eV at the lowest pressure. Band-gap changes with pressure are confirmed with visual observations. $ZrMo_2O_8$ changes from transparent at 5 GPa to yellow at 10 GPa, red at 18 GPa, and at about 30 GPa it becomes opaque.

DOI: 10.1103/PhysRevB.65.064101 PACS number(s): 62.50.+p, 64.70.Kb, 71.30.+h, 63.20.−e

I. INTRODUCTION

In recent years materials that exhibit negative thermal expansion have generated considerable scientific and technological interest. Many studies have been performed on MX_2O_8 and MX_2O_7 (M=Zr and Hf and X=W, Mo, and V), mainly due to their isotropic negative thermal expansion. For example, negative thermal expansion has been reported in ZrW_2O_8,[1] HfW_2O_8,[2] ZrV_2O_7,[3,4] and cubic $ZrMo_2O_8$.[5] It has been proposed that the negative thermal expansion in the tungstates and molybdate is due to the presence of low-frequency rigid modes and in the vanadate it is due to the rotation of the VO_4 tetrahedra.[1,3,4,6] $ZrMo_2O_8$, one of the MX_2O_8 compounds, has several known polymorphs at 1 atm.: γ-$ZrMo_2O_8$ (cubic),[5] α-$ZrMo_2O_8$ (trigonal),[7–9] and β-$ZrMo_2O_8$ (monoclinic).[10] Neutron and x-ray diffraction measurements show that like its structural analog β-ZrW_2O_8, cubic $ZrMo_2O_8$ exhibits isotropic negative thermal expansion, from 11 to 573 K.[5] Unlike ZrW_2O_8, which has an order-disorder phase transition [α (acentric) to β (centric) phase] at 428 K, $ZrMo_2O_8$ does not show a phase transition in this temperature range.[2] A high pressure x-ray diffraction study has found that with compression, cubic $ZrMo_2O_8$ has a phase transition at 0.7–2 GPa with a volume decrease of 11%.[11]

At ambient conditions α-$ZrMo_2O_8$ has the space-group symmetry $P2_13$ with unit-cell parameters $a=10.139$ Å and $c=11.7084$ Å.[8,9] It has a (two-dimensional) 2D network with layers perpendicular to the c axis, which are formed from the ZrO_6 octahedra linked together by MoO_4 tetrahedra. Three of the four oxygen atoms of the molybdate tetrahedra are linked to different Zr atoms. The fourth oxygen atom of each tetrahedron points into the interlayer region and the oxygen atoms form a cubic-close-packed anion arrangement.[7,12] Recently, high pressure x-ray powder diffraction studies by Carlson and Andersen[7] show that at room temperature α-$ZrMo_2O_8$ transforms to δ-$ZrMo_2O_8$ (monoclinic and space-group symmetry $C2/m$) at around 1.1 GPa and another phase transition from the δ phase to the ε phase (triclinic and space-group symmetry $P1$ or $P\bar{1}$) takes place in the pressure range 2 to 2.5 GPa. The unit-cell volume decreases by 4.9% in the α to δ-$ZrMo_2O_8$ phase transition and by 10% over the δ to ε transformation.[7]

In this paper, we report the high-pressure Raman, infrared, and optical absorption spectra of $ZrMo_2O_8$ up to 38 GPa. By the appearance of new vibrational modes in the pressure range 1.1 to 1.3 GPa and 1.9 to 2.3 GPa, Raman and IR spectroscopy reveal two phase transitions.

II. EXPERIMENT

Powder samples of α-$ZrMo_2O_8$ (Ref. 7) were loaded in a Mao-Bell-type diamond-anvil cell. Diamonds with 350 μm culets were used and a spring steel gasket contained the sample. Less than 5% ruby powder was included and used to calibrate the pressure[13] and no pressure transmitting medium was used in the optical-absorption measurements. For the Raman measurements 4:1 methanol:ethanol mixture was used as the pressure transmitting medium. For IR measurements the sample was diluted with KBr powder (1:99) for ambient and (1:20) for high-pressure measurements.

High-pressure optical-absorption measurements in the range 1 to 4 eV were carried out in transmission geometry using a monochromator with a liquid nitrogen cooled photomultiplier tube, and a tungsten-halogen lamp was used as the light source. Spectra were initially collected without the sample to determine the system response. Spectra of the diamond anvils were also collected and used as reference to determine the absorbance of the $ZrMo_2O_8$. Raman measurements were carried out using an OMARS 89 Raman spectrometer equipped with a liquid nitrogen cooled charged-coupled device. The 514.5 nm line of an argon ion laser was used as the excitation source and the scattered light from the sample was collected in the backscattering geometry. Infrared-absorption measurements were carried out using a Nicolet Nexus 670 Fourier transform infrared spectrometer equipped with a liquid nitrogen cooled MCT-A detector.

III. RESULTS AND DISCUSSION

The pressure-induced changes in the Raman active vibrational modes are shown in Figs. 1(a) and 1(b). The spectrum recorded at ambient conditions has eight modes. By compari-

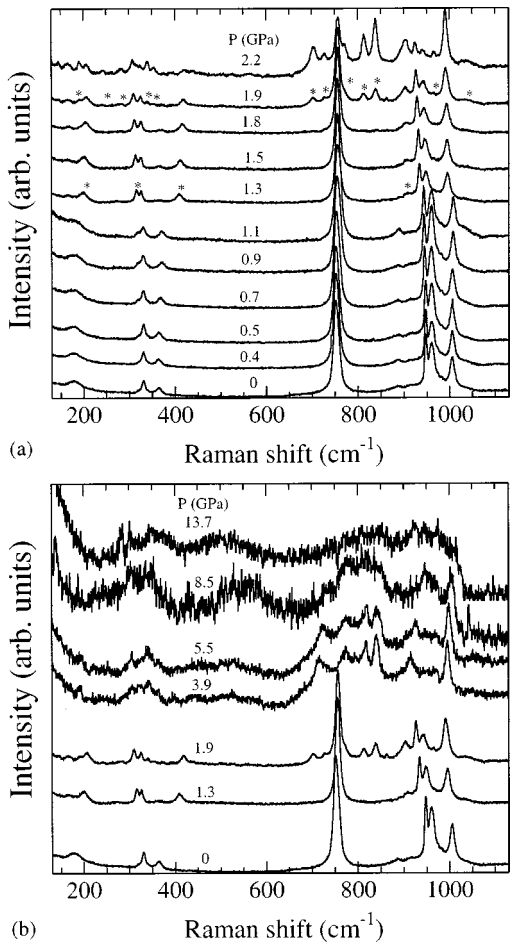

FIG. 1. (a) Raman spectra recorded at various low pressures in the range 130–1130 cm^{-1} for the α, δ, and ε phases of $ZrMo_2O_8$. The symbol * indicates new modes (b) Raman spectra recorded at various high pressures in the range 130–1130 cm^{-1}. The spectrum recorded at 8.5 GPa has broad Raman modes, characteristic of amorphous samples.

son with the spectra of other molybdates[14–16] the strong modes centered at 1003, 960, and 948 cm^{-1} are assigned to the symmetric stretching of MoO_4 tetrahedra and the 887 and 753 cm^{-1} modes are assigned to the asymmetric stretching; those at 364 and 331 cm^{-1} to the MoO_4 symmetric bending and asymmetric bending, respectively; and the peak at 177 cm^{-1} to a lattice mode. With compression the mode at 331 cm^{-1} develops a shoulder and becomes a doublet (317 and 326 cm^{-1}) and the lattice mode at 177 cm^{-1} also becomes a doublet (166 and 199 cm^{-1}) at 1.3 GPa. Two other new modes appear at 409 and 910 cm^{-1} at this pressure [Fig. 1(a)]. These changes can be related to the α to δ-$ZrMo_2O_8$ phase transition that has been observed in high pressure x-ray diffraction measurements, where the crystal structure changes from a higher-symmetry (trigonal) to a lower-symmetry (monoclinic) phase.[7,12]

With increasing pressure, new modes appear at 192, 243, 281, 340, 353, 703, 729, 770, 813, 838, 964, and 1032 cm^{-1} at 1.9 GPa [Fig. 1(a)]. This change is associated with the δ to ε-$ZrMo_2O_8$ phase transition observed in the high-pressure x-ray measurement at 2 GPa.[7] Above ~6 GPa all the modes

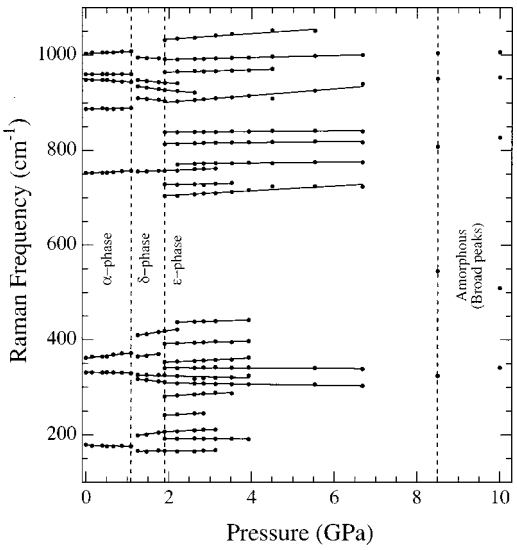

FIG. 2. The pressure dependence of the observed Raman modes.

become weak and start broadening [Fig. 1(b)]. At 8.5 GPa and above, the modes are centered approximately at 324, 545, 807, and 950 cm^{-1} [Fig. 1(b)]. These modes that are present to the highest pressure for which Raman spectra were collected, 23 GPa, demonstrate the existence of the MoO_4 tetrahedra. This is similar to the two broad WO_4 Raman modes observed at 3.5 GPa in amorphous ZrW_2O_8.[17] Thus, we suggest that the mode broadening above 6 GPa may be due to amorphization of $ZrMo_2O_8$ [Fig. 1(b)]. Carlson and Andersen[7] observed a weakening and broadening of the Bragg scattering from $ZrMo_2O_8$ at ~8 GPa, which they attributed to either increasing nonhydrostatic conditions in the diamond-anvil cell or pressure-induced amorphization. Since the pressure-transmitting medium in their experiment (4:1 methanol:ethanol) is hydrostatic to over 10 GPa, we would suggest that the sample is undergoing pressure-induced amorphization.

Figure 2 shows the plot of the Raman frequencies vs pressure. The appearance of new Raman modes at around 1.1 and again at 1.9 GPa further documents the high-pressure phase transformations. The mode Grüneisen parameters, which can be related to the Grüneisen parameter, a key parameter for determining thermal properties, are calculated for the various Raman active modes. The mode Grüneisen parameter γ_i is defined as $\gamma_i=(\omega_i\chi_T)^{-1}(\partial\omega_i/\partial P)$, where ω_i is the frequency of the ith mode, P is the pressure, and χ_T is the isothermal volume compressibility. Table I lists the pressure derivatives and mode Grüneisen parameters of the various Raman mode frequencies of α-, δ-, and ε-$ZrMo_2O_8$. It is noted that some of the lattice modes and the MoO_4 symmetric stretching and bending modes exhibit negative Grüneisen parameters.

Figure 3 shows the vibrational modes measured by infrared spectroscopy at various pressures at room temperature. Due to the experimental limitations only modes above 600 cm^{-1} were recorded. At ambient conditions there are modes centered at 668, 681, 741, 871, 932, 975, and 996 cm^{-1}. With increasing pressure new modes start appearing, espe-

TABLE I. Mode Grüneisen parameters (γ_i) and pressure derivatives ($d\omega/dP$) of the various Raman modes of α-, δ-, and ε-$ZrMo_2O_8$. Reported values of $\chi_T = 5.1\times10^{-2}$, 4.2×10^{-2}, and 1.1×10^{-2} GPa^{-1}, respectively, for the three phases are used in the calculation.[7]

	α (0 GPa)			δ (1.3 GPa)			ε (1.9 GPa)		
Assignment	Mode freq. (cm^{-1})	$d\omega/dP$ (cm^{-1}/GPa)	γ_i	Mode freq. (cm^{-1})	$d\omega/dP$ (cm^{-1}/GPa)	γ_i	Mode freq. (cm^{-1})	$d\omega/dP$ (cm^{-1}/GPa)	γ_i
							1032	5.90	0.52
	1003	4.09	0.08	995	−3.55	−0.08	992	2.03	0.19
$\nu_s(MoO_4)$	960	0	0	948	−7.64	−0.19	964	2.22	0.21
	948	−4.75	−0.10	934	−11.55	−0.29	927	−7.28	−0.71
				910	−8.73	−0.23	904	7.03	0.71
							838	7.03	0.76
							813	0.97	0.11
	887	1.31	0.03				770	0.86	0.10
$\nu_{as}(MoO_4)$	753	4.68	0.12	756	1.29	0.04	757	4.75	0.57
							729	1.51	0.19
							703	5.02	0.65
$\delta_{as}(MoO_4)$	364	9.47	0.51	409	13.09	0.76	437	2.49	0.52
				365	10.01	0.65	392	2.42	0.56
							353	4.24	1.09
							340	−0.33	−0.09
$\delta_s(MoO_4)$	331	−1.50	−0.09	326	−1.85	−0.14	326	−3.36	−0.94
				317	−9.46	−0.71	311	−1.25	−0.36
							281	4.50	1.46
							243	4.52	1.69
				199	12.16	1.45	207	4.11	1.81
Lattice modes	177	−2.25	−0.25				192	−0.41	−0.19
				166	0.77	0.11	166	1.50	0.82

cially in the 760 cm^{-1} region. This change is similar to the new modes observed in the Raman spectra around 1 GPa where the α- to δ-$ZrMo_2O_8$ phase transition takes place.[7] With further compression a new mode appears around 800 cm^{-1} and it is clearly visible at 2.8 GPa. This change may be related to the new modes observed in the Raman spectra around 2 GPa, the pressure for the δ- to ε-$ZrMo_2O_8$ phase transition.[7] Table II lists infrared frequencies of α-, δ-, and ε-$ZrMo_2O_8$. Figure 4 shows the pressure dependence of the infrared frequencies.

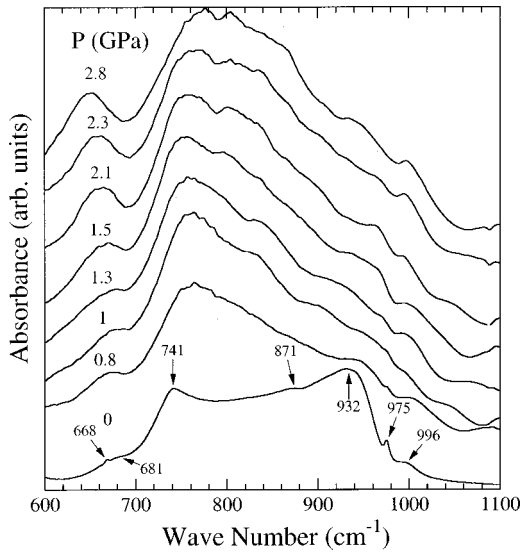

FIG. 3. A series of infrared absorption spectra recorded at various pressures.

Representative transmission spectra, normalized to the reference spectrum are shown in Fig. 5(a). The spectra clearly show the change in transmission with pressure. After ratioing to the reference spectrum, the transmitted light through the sample yields the absorbance of the sample [the absorbance is the absorption coefficient (α) times the sample thickness (t)]. Assuming parabolic conduction and valence bands, as well as a direct band gap, a plot of $(\alpha tE)^{1/2}$ vs incident photon energy (E) should yield a straight line in the high energy regions of the spectrum [Fig. 5(b)], where the contribution to the absorption coefficient due to other mechanisms is negligible. With these assumptions, an extrapolation of the linear portion to zero absorption yields the band gap.[18,19] If $ZrMo_2O_8$ has an indirect band gap, then the actual band gap at each pressure is slightly off from the band-gap energy quoted here.[20] The color of the sample directly indicates the changes in the band gap. The initially pink sample becomes transparent at 5 GPa, yellow around 10 GPa, red around 18 GPa, and by 30 GPa the central region of the sample becomes opaque, although the outer rim, which is at a lower pressure, is still red.

TABLE II. Infrared frequencies (cm^{-1}) of $ZrMo_2C_8$ of the α (trigonal), δ (monoclinic), and ε (triclinic) phases

Assignment	α (0 GPa)	δ (1 GPa)	ε (2.3 GPa)
	996	998	996
$\nu_s(MoO_4)$	975	976	966
	932	956	932
		902	902
	871		867
		831	837
		774	804
$\nu_{as}(MoO_4)$		762	771
		754	757
	741	747	746
	681	673	657
	668		

Figure 6 shows the estimated band gap vs pressure. At the lowest pressure (~0 GPa) the estimated band gap is 0.6 eV. Up to a pressure of 1.3 GPa the band gap changes from 0.6 to ~0.3 eV. Above 1.3 GPa the band gap starts increasing until it reaches a maximum of 1.4 eV at around 11 GPa. Above this pressure the band gap starts decreasing with increasing pressure, reaching 0.9 eV at 38 GPa.

At about 1 GPa, $ZrMo_2O_8$ undergoes a structural phase transition (α to δ). The α and δ phases have volume compressibilities of 5.1×10^{-2} and $4.2\times10^{-2}\,GPa^{-1}$, respectively.[7,12] The compressibility is larger in the *c* direction and the applied pressure is mainly accommodated by decreasing the interlayer distance instead of compressing the Zr-O and Mo-O bonds.[12] Since the bond lengths of the polyhedra do not change significantly in this pressure regime the application of pressure would be expected to increase the bandwidths of the bands without affecting the band center thus, leading to a reduction in the band gap with pressure.

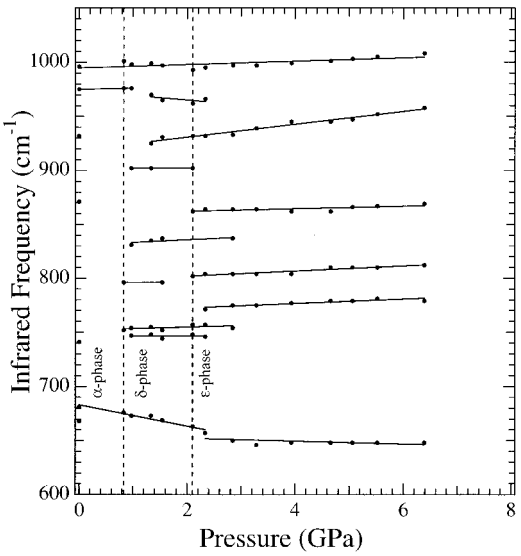

FIG. 4. The pressure dependence of the observed infrared frequencies.

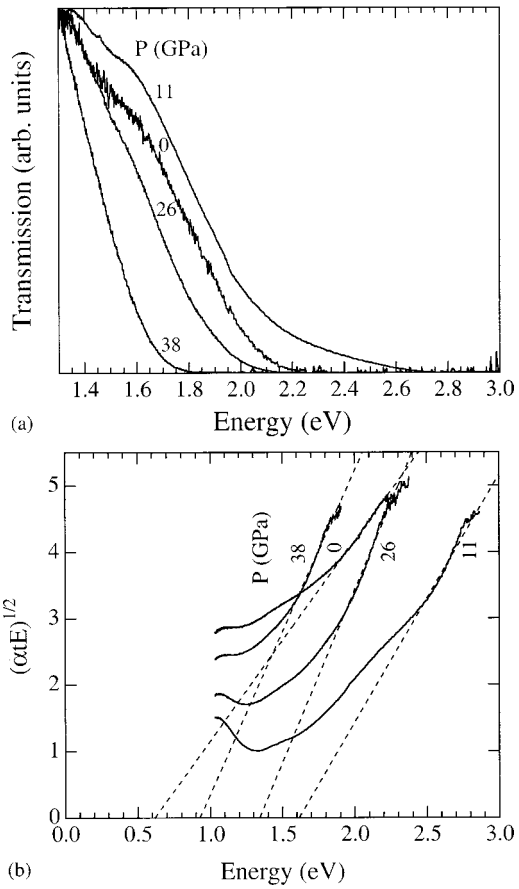

FIG. 5. (a): Representative plots of transmission vs incident photon energy for various pressures. (b): The solid lines are graphs of $(\alpha tE)^{1/2}$ (α – absorption coefficient, t – sample thickness) vs the incident photon energy (E), for various high pressures. The dashed lines are the linear fits to the high energy region, and the band gap is determined by extrapolating the fit to zero absorption.

Similar pressure effects are observed in high-pressure band-gap measurements of As_2S_3[21,22] and GaTe.[23]

At about 1.3 GPa, the band gap increases and reaches a maximum of 1.4 eV at around 11 GPa. In this pressure re-

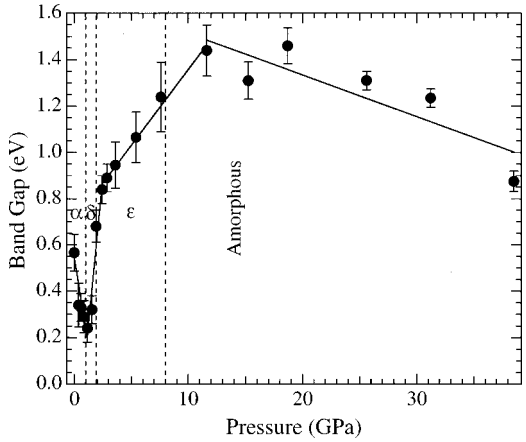

FIG. 6. The band gap of $ZrMo_2O_8$ vs pressure on compression. The solid lines between 0 to 11 GPa are guides to the eye. The solid line from 11 to 38 GPa is a linear least-squares fit to the data.

gime $ZrMo_2O_8$ is in the triclinic ε phase. The ε phase has a volume compressibility of $1.1\times10^{-2}\,\mathrm{GPa}^{-1}$ which is 4–5 times less than the α and δ phases, and is more densely packed than the other two phases.[7] We speculate that for the ε phase, the applied pressure may alter the centers of the conduction and valence bands as well as the bandwidths. It may be that the shift of the band centers is greater than the broadening of the bandwidths, leading to an overall increase in the band gap as in the case of the layered semiconductor GaTe and tetragonally bonded amorphous Ge, Si, and GaAs.[23,24] The discontinuities in the slope of the band gap at 1 and 2 GPa may be due to the α to δ and the δ to ε phase transitions (Fig. 6).

Above ~11 GPa, when the $ZrMo_2O_8$ is amorphous the band gap again starts decreasing with pressure at a rate of -0.018 ± 0.005 eV/GPa. A linear extrapolation indicates that $ZrMo_2O_8$ will become a metal at around 90 GPa.

IV. CONCLUSION

In conclusion, we report Raman, IR, and optical-absorption measurements for the three crystal structures (α, δ, and ε) and for noncrystalline $ZrMo_2O_8$ under high pressure. Raman and IR spectroscopy document the previously identified phase transitions from the α (trigonal) to the δ (monoclinic) phase at 1 GPa and the δ to the ε (triclinic) phase at 1.9 GPa, through the appearance of new modes and discontinuities in the slopes of other modes. Additionally, Raman spectroscopy supports the ε to amorphous $ZrMo_2O_8$ transition at ~8.5 GPa. Optical-absorption measurements show a small decrease in the band-gap energy below 1.3 GPa, an increase of about 1.2 eV between 1.3 to 11 GPa and a linear decrease above 11 GPa. It would be interesting to calculate the band structure of $ZrMo_2O_8$ under compression to get additional insight into the behavior of the band gap with pressure.

ACKNOWLEDGMENT

This work was supported by the National Science Foundation and the Petroleum Research Fund.

[1] T. A. Mary, J. S. O. Evans, T. Vogt, and A. W. Sleight, Science **272**, 90 (1996).
[2] J. S. O. Evans, T. A. Mary, T. Vogt, M. A. Subramanian, and A. W. Sleight, Chem. Mater. **8**, 2809 (1996).
[3] V. Korthuis, N. Khosrovani, A. W. Sleight, N. Roberts, R. Dupree, and W. W. Waren, Chem. Mater. **7**, 412 (1995).
[4] A. K. A. Pryde, K. D. Hammonds, M. T. Dove, V. Heine, J. D. Gale, and M. C. Warren, J. Phys.: Condens. Matter **8**, 10 973 (1996).
[5] C. Lind, A. P. Wilkinson, Z. Hu, S. Short, and J. D. Jorgensen, Chem. Mater. **10**, 2335 (1998).
[6] H. Volker and R. L. Patrick, J. Am. Ceram. Soc. **82**, 1793 (1999).
[7] S. Carlson and A. M. K. Andersen, Phys. Rev. B **61**, 11209 (2000).
[8] M. Auray, M. Quarton, and P. Tarte, Acta Crystallogr., Sect. C: Cryst. Struct. Commun. **42**, 257 (1986).
[9] V. N. Serezhkin, V. A. Efremov, and V. K. Trunov, Russ. J. Inorg. Chem. **32**, 1566 (1987).
[10] M. Auray, M. Quarton, and P. Tarte, Powder Diffr. **2**, 36 (1987).
[11] C. Lind, D. G. VanDerveer, A. P. Wilkinson, J. Chen, M. T. Vaughan, and D. J. Weidner, Chem. Mater. **13**, 487 (2001).
[12] A. M. Krogh Andersen and S. Carlson, Acta Crystallogr., Sect. B: Struct. Sci. **57**, 20 (2001).
[13] H. K. Mao, P. M. Bell, J. W. Shaner, and D. J. Steinberg, J. Appl. Phys. **49**, 3276 (1978).
[14] M. Maczka, J. Solid State Chem. **129**, 287 (1997).
[15] M. S. Augsburger and J. C. Pedregosa, J. Phys. Chem. Solids **56**, 1081 (1994).
[16] A. Jayaraman, S. Y. Wang, and S. K. Sharma, Solid State Commun. **93**, 885 (1995).
[17] C. A. Perottoni, and J. A. H. da Jornada, Science **280**, 886 (1998).
[18] J. Tauc, R. Grigorovici, and A. Vancu, Phys. Status Solidi **15**, 627 (1966).
[19] A. F. Goncharov, E. Gregoryanz, H. K. Mao, Z. Liu, and R. J. Hemley, Phys. Rev. Lett. **85**, 1262 (2000).
[20] J. I. Pankove, *Optical Processes in Semiconductors* (Dover Publications, New York, 1975).
[21] B. A. Weinstein, R. Zallen, and M. A. Slade, J. Non-Cryst. Solids **35&36**, 1255 (1980).
[22] R. Zallen, *The Physics of Amorphous Solids* (Wiley, New York, 1983).
[23] J. Pellicer-Porres, F. J. Monjon, A. Segura, and V. Munoz, Phys. Rev. B **60**, 8871 (1999).
[24] S. R. Elliot, *Physics of Amorphous Materials* (Longman, London, 1983).